NOTES AND CORRESPONDENCE

High-Resolution Observations of Mammatus in Tropical Anvils

PAVLOS KOLLIAS, IENG JO, AND BRUCE A. ALBRECHT

Division of Meteorology and Physical Oceanography, University of Miami, Miami, Florida

(Manuscript received 30 June 2004, in final form 4 October 2004)

ABSTRACT

Unprecedented high-resolution observations of mammatus from a profiling 94-GHz Doppler radar during the NASA Cirrus Regional Study of Tropical Anvils and Cirrus Layers–Florida Area Cirrus Experiment (CRYSTAL–FACE) are presented. Because of its high sensitivity and temporal and spatial resolution, the cloud radar used was able to resolve the fine structure of individual mammatus clouds and record significant vertical Doppler velocity perturbations (-6 to $+1$ m s^{-1}). Strong perturbations of the Doppler velocity within the mammatus as it extends below the main cirrus cloud base are captured by the radar observations. Upward motions in the periphery of descending mammatus cores are documented. Areas of intense, small-scale turbulent mixing near the cirrus cloud base are identified using the Doppler spectrum width. Power spectra analysis of the mean Doppler velocity field supports the presence of gravity waves and the development of higher-frequency structures near the cirrus anvil base, where the mammatus clouds are observed. The observations provide strong evidence for dynamical forcing from coherent vertical motions 500 m above the cloud base contributing to the mammatus formation. The results are discussed in the context of suggested theories for mamma formation and morphology.

1. Introduction

Mammatus clouds frequently form on the base of convective anvils and middle-level cirrus generated by deep cumulonimbus. Mammatus clouds are often described as pouches with smooth outlined surfaces hanging down from the cloud base (Scorer 1958). Because of their notable visible appearance, mammatus capture the interest of scientists and photographers (e.g., Stith 1995; Warner 1973). Scorer (1958) identified three possible main mechanisms for the production of mamma: subsidence of a cloud interface layer, fallout of precipitation, and evaporation of precipitation. These processes, when present near the cloud base, can result in temperature discontinuities and thus instability that can produce moderate downdrafts and furthermore explain the smooth appearance of mammatus clouds. Martner (1995), however, reported that the formation of mammatus clouds is not a cloudy–clear air interfacial process and that the root of the mammatus clouds are deep in the cloud layer where evaporation is not likely to occur. Martner and others (e.g., Clarke 1962; Winstead et al. 2001) suggest that gravity and Kelvin–Helmholtz waves contribute to mammatus clouds' formation. Another unanswered question is the level of turbulence in the vicinity of mammatus. Mammatus clouds are often associated with the presence of high atmospheric turbulence levels and severe weather conditions that can be hazardous for aviation. However, the majority of past observations suggest that turbulence is weak in the vicinity of mammatus clouds. Furthermore, the role of large ice crystals in mamma production is unclear.

Radar measurements of mammatus characteristics have been extremely scarce. Only two cases of radar observations of mamma clouds have been reported, one by ground-based Doppler radar (Martner 1995) and another by airborne Doppler radar (Winstead et al. 2001). These past radar measurements have advanced our knowledge of mamma clouds. However, they lack the resolution needed to resolve the small-scale features of mammatus clouds.

In this study, high-resolution radar observations of mammatus clouds were made to examine the small-

Corresponding author address: Dr. Pavlos Kollias, RSMAS/MPO, 4600 Rickenbacker Causeway, Miami, FL 33149-1096.
E-mail: kollias@rsmas.miami.edu

scale features of mammatus clouds. These observations were made during the National Aeronautics and Space Administration's (NASA) Cirrus Regional Study of Tropical Anvils and Cirrus Layers–Florida Area Cirrus Experiment (CRYSTAL–FACE) conducted in south Florida on 22 July 2002. Deep oceanic convection east of the central Florida coast produced widespread cirrus outflow. The mammatus observations were collected by the University of Miami 94-GHz Doppler Cloud Radar (UMDCR; Albrecht et al. 1999) as the 6-km-thick cirrus cloud advected over a radar ground site located at Tamiami Airport, 25 km southwest of Miami. The vertically pointing UMDCR recorded 512 FFT-point Doppler spectra obtained with a 5-kHz pulse repetition frequency (± 4 m s^{-1} Nyquist velocity). The vertical resolution was 30 m and the temporal resolution 1.7 s. The sensitivity of the UMDCR during the experiment was estimated at -51 dBZ at 1 km for 1-s averaging. These high-resolution radar observations provide important, detailed radar images of mammatus clouds and document interesting dynamical features that will be used to address issues concerning the formation of mammatus clouds.

2. Observations

The first three Doppler moments of the UMDCR observations were calculated from the recorded Doppler spectra, and a cloud mask was applied using the cloud reflectivity. Figure 1 shows 4 h of time–height mapping of the cirrus cloud reflectivity, mean Doppler velocity, and Doppler spectrum width from the UMDCR. At the beginning of the observing period, the parent cirrus anvil cloud top was around 14 km and gradually descended to less than 10 km after 5 h of observations (Fig. 1). The anvil reflectivity structure exhibits finescale features near the cloud top. A wide area of high reflectivity (large ice crystals signature) descends near the cloud base after the first 2 h of observations. At 0230 UTC, mammatus clouds are observed at the cloud base by the UMDCR. The zero temperature isotherm is at 4.3-km height, as melting of ice crystal at this altitude was observed at the late stage of the observations (0500 UTC; not shown). Gravity wave activity (barlike features in Fig. 1, middle panel) imbedded with the ice crystals' sedimentation velocities ($\sim$0.5–1.0 m s^{-1}) and shallow layers with turbulence signatures manifested in the Doppler spectrum width observations (Kollias et al. 2001) were well defined by the UMDCR. Earlier in the observing period (0030–0200 UTC), the shallow turbulent area is well above the cloud base (narrow band of high spectral widths around 7 km). During that period, no mammatus clouds were formed despite the presence of a large descending high-reflectivity core. The mammatus form at the cirrus base when another broad area of high ice crystal reflectivity (dBZ$>$0) reached the cloud base (0215 UTC). The layer of high spectra width values descended near the cloud base just before the onset of the mammatus formation. For this study, the analysis of the waves defined by the vertical mean Doppler velocity is limited to the anvil area where the mammatus formed.

Figure 2 shows the mean Doppler velocity $<V_z>$ (m s^{-1}) and the Doppler spectrum width σ_v (meters per second) from the UMDCR within the box area indicated in Fig. 1. The observations cover a 25-min period. Several mammatus clouds at different stages of development at the cirrus base are displayed. The temporal scale of the mammatus oscillations is around 1 min. The mamma periphery is characterized by low reflectivity values. The UMDCR sensitivity is better than -30 dBZ at this altitude. Following the cloud boundaries, it is apparent that at the mamma area the cloud base undulates by 200–600 m and the reflectivity exhibits a sharp decrease near the mammatus cloud boundaries. The reflectivity measurements (not shown) exhibit no structure above the undulating cloud base. The higher Doppler moments shown in Fig. 2, however, reveal a different picture. The mean Doppler velocity, which is the sum of the vertical air motion and the reflectivity-weighted ice crystals fall velocity, shows evidence of mammatus organization to about 500 m above the cirrus base with narrow downdraft structures that develop in mature (extending below the mean cloud base) mammatus.

Doppler velocities of -3 to -5 m s^{-1} are observed in the mammatus. Near the mamma fronts (bases) the magnitude of the downdrafts decreases significantly, indicating the presence of either updrafts or smaller ice crystals. The highest mean Doppler velocities (slightly downward or even upward) are observed at the mamma sides and are highly correlated with low reflectivity values. Above 6.5 km, ice crystal fall velocities are the primary contributor to σ_v, and typical values of σ_v are between 0.2 and 0.3 m s^{-1}. Near the cloud base and within the mammatus clouds, the Doppler spectrum width mapping reveals interesting fine structure layers with σ_v values higher than 0.6–0.7 m s^{-1}. The Doppler spectrum width σ_v parameter can be used to retrieve the turbulence dissipation rate ε (cm^2 s^{-3}). Away from wind shear zones, the main contributors to the observed Doppler spectrum width σ_v are the breath of the ice crystals size distribution σ_{DSD} and radar subresolution volume turbulence σ_t (Kollias et al. 2001). Using

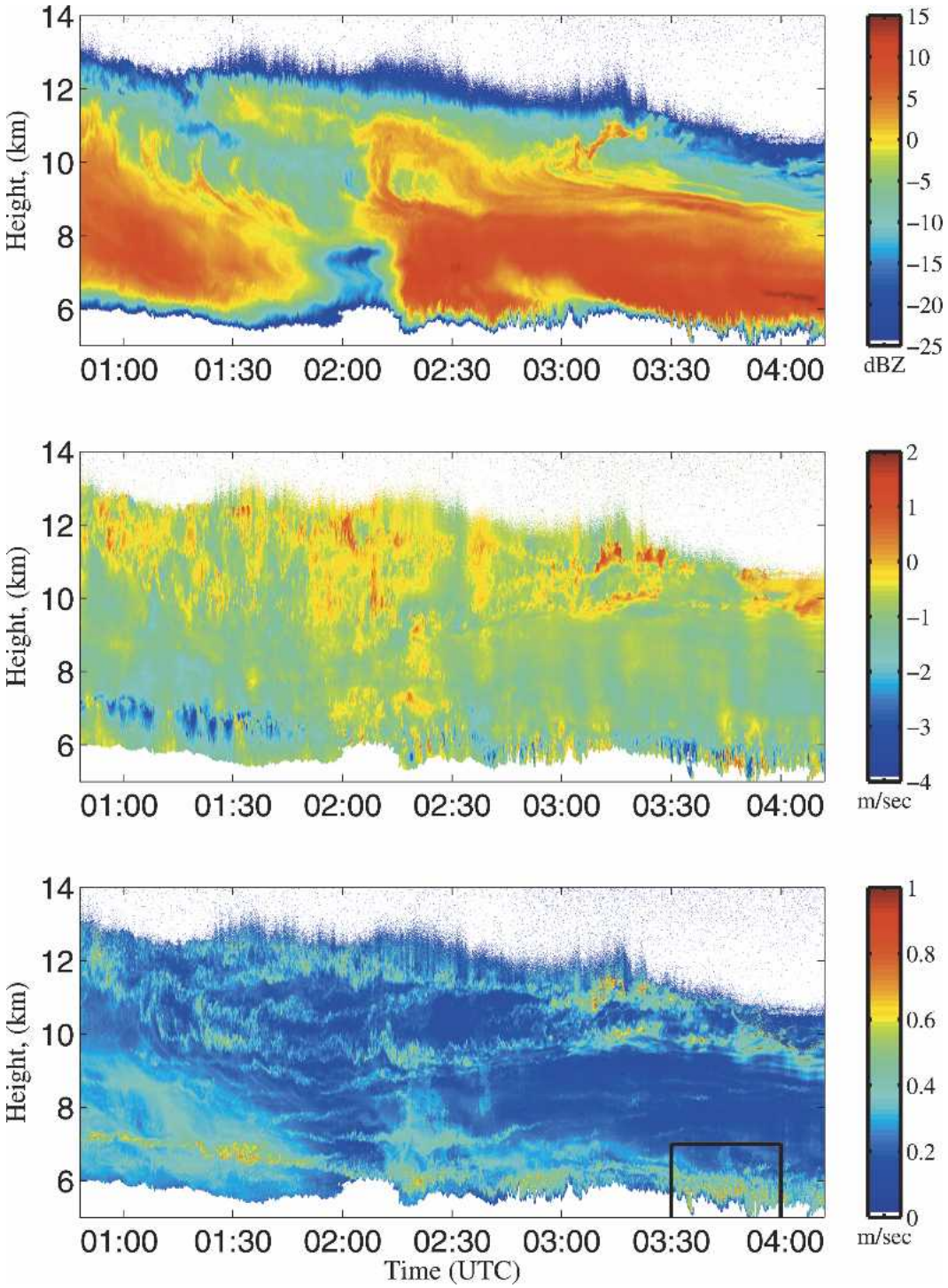

FIG. 1. (top) Time–height mapping of radar reflectivity, (middle) mean Doppler velocity (m s^{-1}), and (bottom) Doppler spectrum width (m s^{-1}) of the cirrus cloud that produced the mammatus clouds. The box indicates the area analyzed in detail in this study.

the mean value of σ_v above the mammatus region (0.2 m s^{-1}) as a proxy for σ_{DSD}, the parameter σ_t is retrieved and the dissipation rate ε (cm^2 s^{-3}) is given by $A\sigma_t^3$, where A depends on the radar characteristics (e.g., range, antenna bandwidth, pulse width) and for the UMDCR at 6-km height is 4.78×10^{-3} m^{-1}. Thus, Doppler spectrum width value of 0.6, 0.8, and 1.0 m s^{-1} corresponds to 86, 220, and 450 cm^2 s^{-3} of turbulence

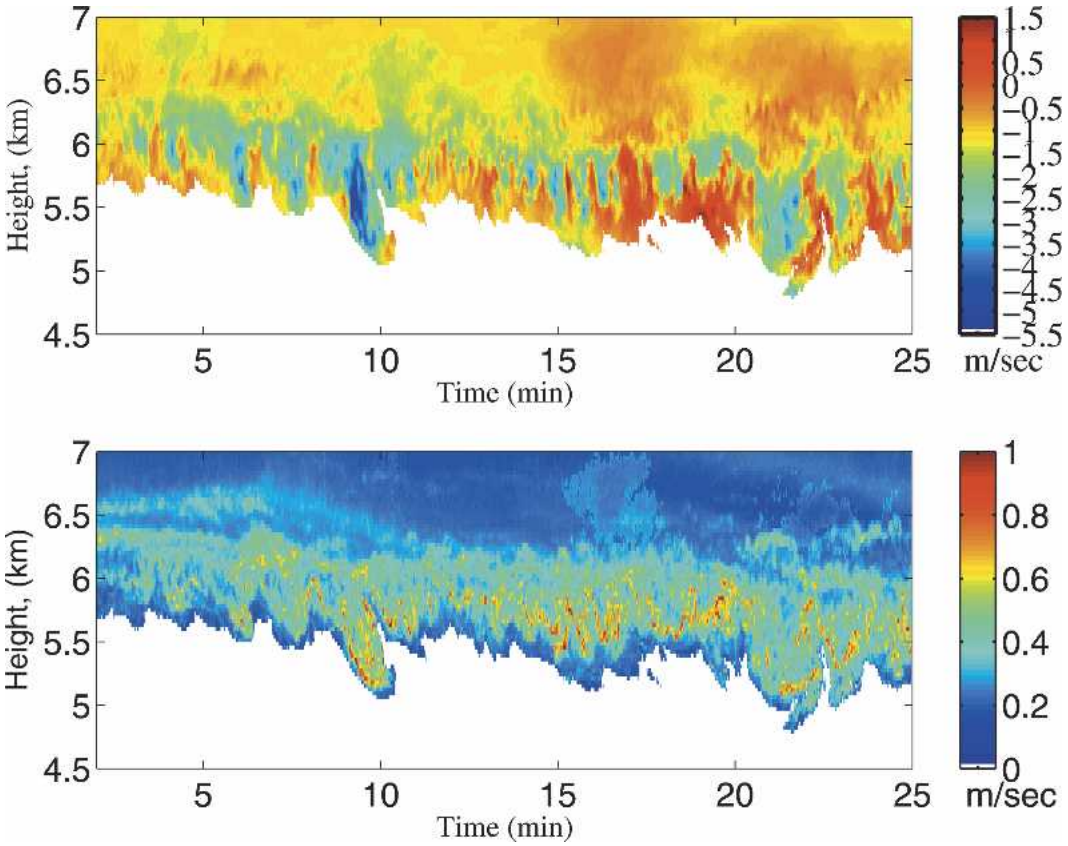

FIG. 2. High-resolution observations of (top) mammatus mean Doppler velocity and (bottom) Doppler spectrum width from the UMDCR.

dissipation rate. This suggests the presence of areas in mammatus cloud that are highly turbulent.

Higher within the deep cirrus layer and above the area of mammatus development, long wavelength gravity waves are observed by the mean Doppler velocity field (see Fig. 1). Using the mean Doppler velocity observations from 0230–0400 UTC and 6–9-km altitude, the profile of the variance of the mean Doppler velocity and the power density spectra of the mean Doppler velocity field at certain altitudes are shown in Fig. 3. Between 7 and 9 km the variance of the mean Doppler velocity shows little variability, with most of the energy confined at low frequencies ($2 \times 10^{-3} - 3 \times 10^{-3}$ Hz). Near the cloud base, however, the variance of the mean Doppler velocity increases and the power spectra analysis of the mean Doppler velocity at 6.5 and 6.0 km shows energy at higher frequencies with distinct spectral peaks at $7 \times 10^{-3} - 10^{-2}$ Hz. These temporal scales match up with the scales of mammatus clouds at cloud base. The slope of the power spectrum $fS(f)$ in the inertial subrange is closed to –2 (dashed line in Fig. 3). The spectral signature of the low-frequency gravity waves is detected in all heights within the cirrus layer.

3. Individual mamma cloud structure

The high vertical and horizontal variability of the reflectivity and mean Doppler velocity within individual mamma undulation are shown in Fig. 4. Two of the most pronounced mamma clouds were sampled by the radar at $t = 9$ min and $t = 22$ min (see Fig. 2). Displayed are the profiles (not averages) of the cloud reflectivity and mean Doppler velocity within the first mamma core (top) and the cloud and mean Doppler velocity from the interior and periphery of the second mamma (bottom).

The top panel of Fig. 4 shows an unprecedented change of the mean Doppler velocity from -1 to -5 m s^{-1} within 0.7 km of descent, accompanied by a very sharp deceleration near the mamma base. During the downward acceleration the UMDCR reflectivity varies little, suggesting that dynamics rather than particle size is responsible for the sharp vertical gradient of the mean Doppler velocity. However, near the mamma base the increase of the mean Doppler from –5 to –2 m s^{-1} is correlated with a sharp decrease of the reflectivity. Moreover, mean Doppler velocities of -5 m s^{-1}

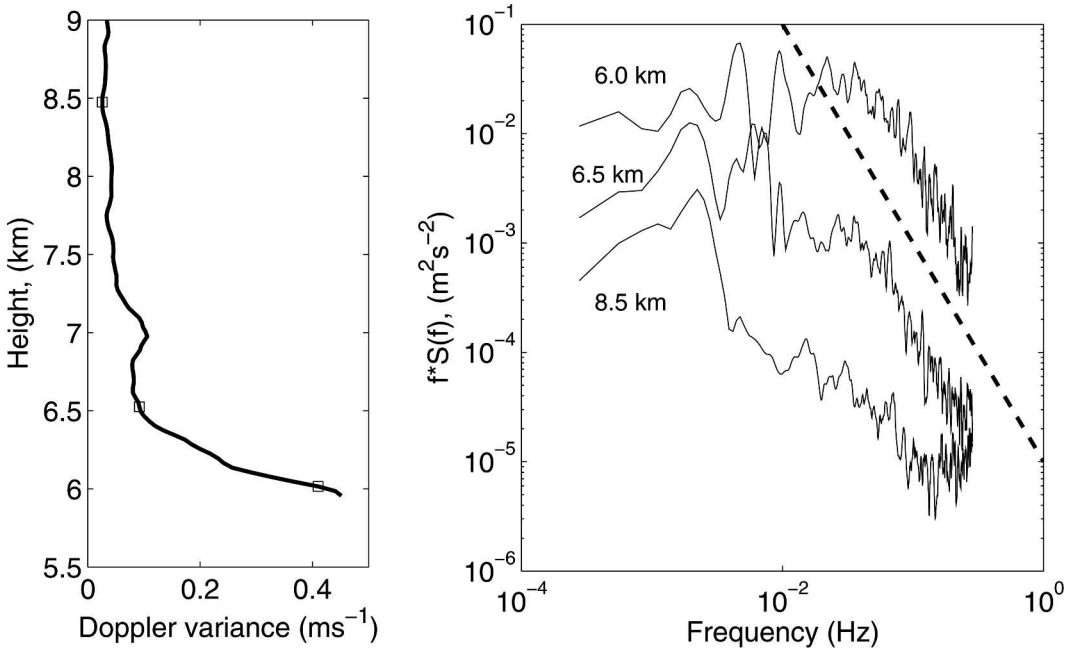

FIG. 3. (left) Vertical profile of the variance of the mean Doppler velocity and (right) examples of power density spectra of mean Doppler velocity time series at 6.0, 6.5, and 8.5 km. The dashed line shows the −2 power law.

observed at ~5.5 km cannot be attributed to ice crystal fall velocities or melting (the 0°C level is at ~4.3 km). If the sharp deceleration in the vertical velocity near the base of the mamma is attributed to the presence of unfavorable thermodynamic environment, the initial descent and acceleration could be attributed to the coherent vertical motion structures that exist near the cloud base.

The bottom panels of Fig. 4 show profiles of cloud reflectivity and mean Doppler velocity in the core and the periphery of the second mamma. A sharp horizontal gradient of cloud reflectivity from the interior to the side of the mamma (~15 dBZ) is present. Furthermore, a sharp horizontal gradient of the mean Doppler velocity is observed. The mean Doppler velocity varies from -4 m s^{-1} in the mamma interior to $+1.5$ m s^{-1} at the side of the mamma cloud.

Figure 5 shows the time–height mapping of reflectivity and mean Doppler velocity field of the second mature mamma entity observed at t = 22 min (Fig. 2). The vertical extent of the mamma entities is used as an indicator of age. The horizontal extent of this mammatus clouds is larger than earlier stage mammatus clouds. A flattening of the mammatus descending front is observed. The reflectivity is higher in the mamma interior and decreases sharply as we approach the cloud boundaries. The mean Doppler velocity field shows coherent vertical velocity structures with strong evidence of recirculation and the presence of updrafts at the mammatus periphery.

4. Discussion

In this paper unprecedented high-resolution observations of mammatus from a profiling W-band Doppler radar during CRYSTAL-FACE are presented. The mammatus production area is placed in the context of the general cirrus cloud morphology and wave and turbulence activity. Cirrus anvils are often embedded in gravity waves generated by the convective activity source. However, not all anvils produce mammatus clouds. In our case, gravity waves are observed throughout the depth of the cirrus clouds, but their scales are not consistent with the mammatus perturbations. The UMDCR observations (Fig. 1) document the presence of a turbulent shallow layer, 500–700 m above the anvil base consistent with the production of mammatus clouds below. This layer produced energy at turbulence scales ($8 \times 10^{-3} - 10^{-2}$ Hz) that are manifested in Fig. 2 as coherent strong updraft and downdraft structures. The vertical velocity magnitude of these structures is greater than the ice crystals' fall velocities, and it is suggested that ice crystal sorting is induced. The ice crystal sorting can result in preferential areas of ice crystal fallout. The origin of this shallow layer is difficult to investigate without other supplementary ob-

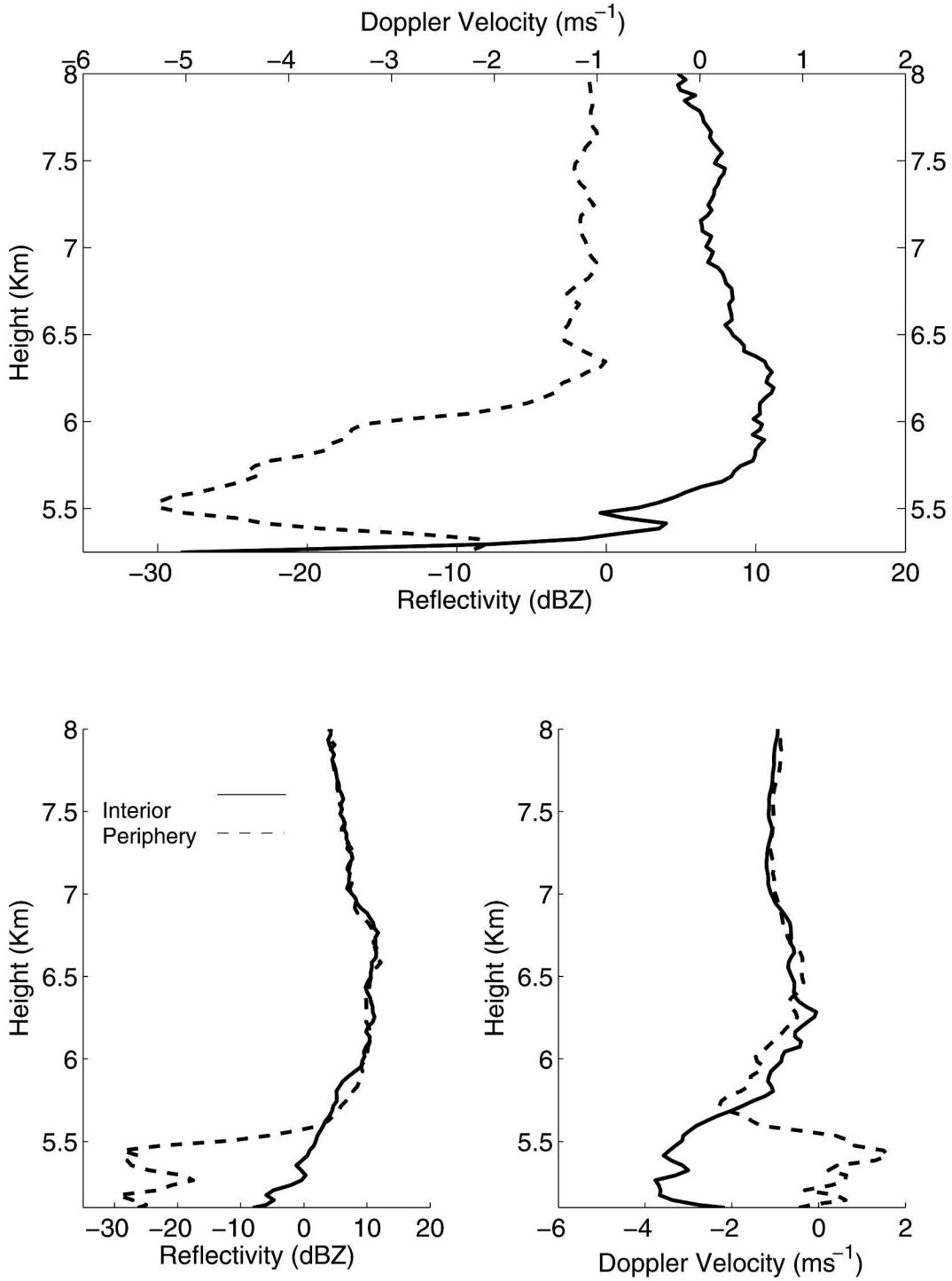

FIG. 4. Profiles of cloud reflectivity and mean Doppler velocity. (top) The interior of the mamma cloud observed at $t = 8.5$ min (see Fig. 2) and (bottom) profiles of cloud reflectivity and mean Doppler velocity collected 30 s apart at $t = 22$ min at the interior (dashed) and side (solid) of the mamma.

servations (the local sounding had bad quality and missing wind data). We suggest that the presence of a source of coherent vertical motions near the cloud base could be key to mammatus formation. This hypothesis is supported by the descending of the layer of high turbulence near the cloud base (Fig. 1) prior to the mammatus formation. Mammatus could be triggered when such intense turbulent mixing areas with small-scale coher-

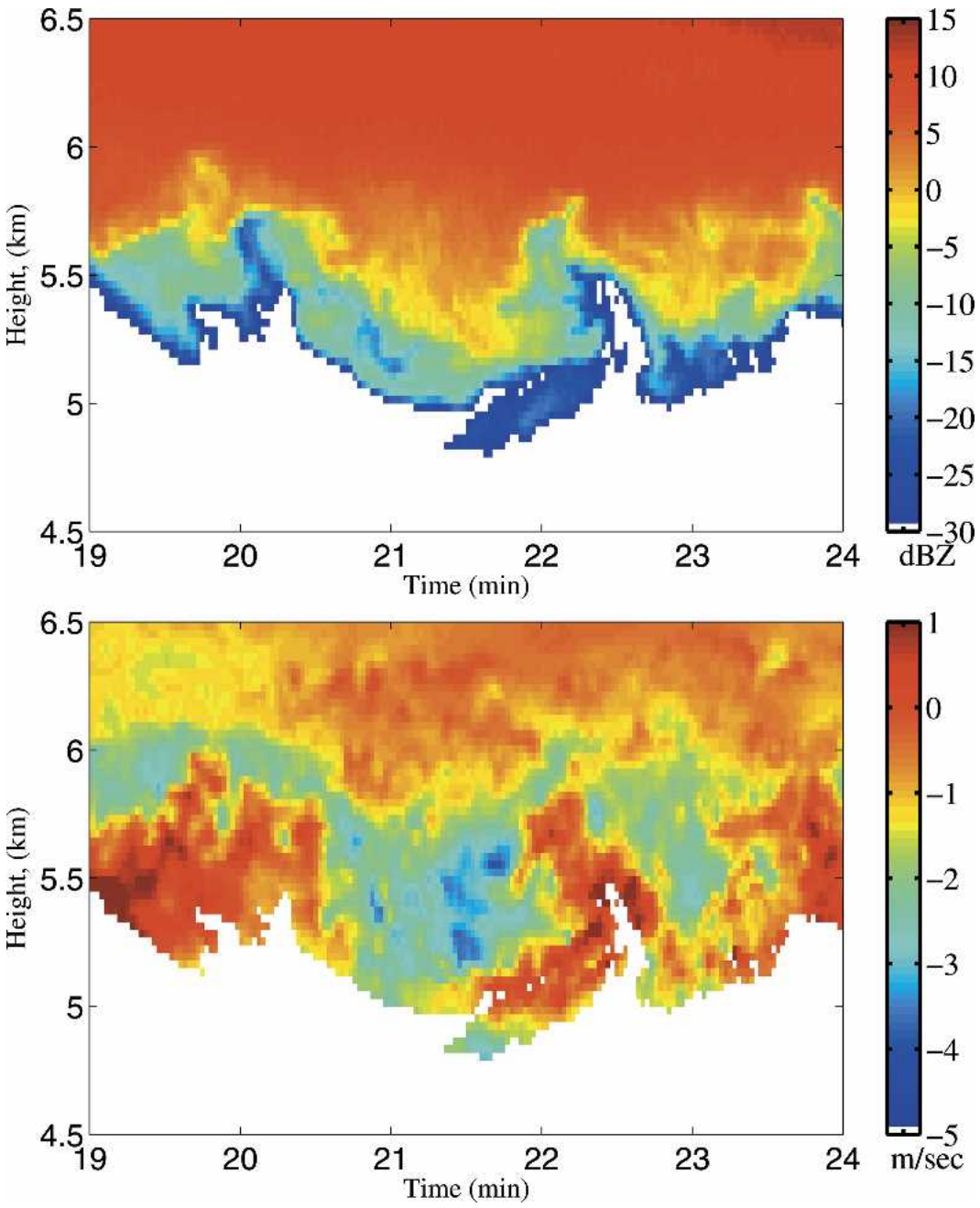

FIG. 5. High-resolution mapping of (top) cloud reflectivity (dBZ) and (bottom) mean Doppler velocity (m s^{-1}) of the mature mamma cloud observed at t = 22 min (see Fig. 2).

ent vertical motions that match the scales of mammatus clouds reach the base of the cloud. While the thermodynamic stability below the cirrus base is not known, the observations presented here provide strong evidence that mechanical processes above the air–cloud interface could force mammatus elements downward even in the absence of thermodynamic instability. Martner (1995) also observed similar turbulent layer and suggested that the root of the mammatus clouds is deep in the cloud.

Layers of high turbulence due to buoyancy and shear instabilities are often encountered in the atmosphere, and cloud droplets or ice crystals can be used by centimeter and millimeter wavelength radars as tracers for their detection (see Doppler spectrum width in Fig. 1). Furthermore, within the mammatus vicinity, areas of

intense mixing involving cloudy and subcloud air are identified using the Doppler spectrum width. The Doppler spectrum width measurements and the retrieved turbulence dissipation rates, along with the significant mean Doppler velocity gradients recorded, suggest that mammatus clouds are highly turbulent. Previous observations provided evidence either for no significant turbulence levels (e.g., Winstead et al. 2001) or for significant turbulence levels (Hlad 1944) in mamma regions. The radar observations presented here have the highest resolution yet, and utilize measurements of the Doppler spectrum width that provide information on the turbulence intensity at scales smaller than the radar resolution volume. The observations demonstrate that the mammatus region has the highest turbulence levels in the cloud and could be hazardous for aviation.

The fine structure of individual mammatus entities is analyzed. The mamma exhibit temporal scales of 1 min (0.6–1.0-km horizontal extent for typical wind speeds at this height) and 0.5–0.7 km vertical extend. The reflectivity and mean Doppler velocity measurements show sharp horizontal gradients. Strong downward mean Doppler velocities (4–5 $m\,s^{-1}$) are observed in the mamma cores and compensating upward motions (1–2 $m\,s^{-1}$) are observed in the mamma peripheries. The mature mamma radar image (Fig. 5) shows a widening of the mamma base as the larger ice particles enter the dry subcloud air and overturning around the edges of the mamma. This is consistent with early theories (e.g., Hlad 1944; Scorer 1958) for the smooth appearance of mammatus clouds once they develop.

Finally, the observations demonstrate the capability of the UMDCR and 94-GHz radars in general to capture the fine structure of cloud structures and highlight important cloud-scale processes often undersampled by other active sensors.

Acknowledgments. This work was supported by NASA CRYSTAL-FACE Grant NAG511508 and NSF Grant ATM 0201072. The contributions of Mr. Tom Snowdon on the development and deployment of the UMDCR are greatly appreciated.

REFERENCES

Albrecht, B., P. Kollias, R. Lhermitte, and R. Peters, 1999: Observations of tropical cloud systems with a MM-wavelength Doppler radar—An overview. Preprints, *29th Int. Conf. on Radar Meteorology,* Montreal, QC, Canada, Amer. Meteor. Soc., 454–456.

Clarke, R. H., 1962: Pressure oscillations and fallout downdraughts. *Quart. J. Roy. Meteor. Soc.,* **88,** 459–469.

Hlad, C. J., Jr., 1944: Stability tendency and mammatocumulus clouds. *Bull. Amer. Meteor. Soc.,* **25,** 327–331.

Kollias, P., B. A. Albrecht, R. Lhermitte, and A. Savtchenko, 2001: Radar observations of updrafts, downdrafts, and turbulence in fair weather cumuli. *J. Atmos. Sci.,* **58,** 1750–1766.

Martner, B. E., 1995: Doppler radar observations of mammatus. *Mon. Wea. Rev.,* **123,** 3115–3121.

Scorer, R. S., 1958: The dynamics of Mamma. *Sci. Prog.,* **46,** 75–82.

Stith, J. L., 1995: In situ measurements and observations of cumulonimbus mamma. *Mon. Wea. Rev.,* **123,** 907–914.

Warner, C., 1973: Measurements of mamma. *Weather,* **28,** 394–397.

Winstead, N. S., J. Verlinde, S. T. Arthur, F. Jaskiewicz, M. Jensen, N. Miles, and D. Nicosia, 2001: High-resolution airborne radar observations of mammatus. *Mon. Wea. Rev.,* **129,** 159–166.